

1 **Enhancing the darkside: Asymmetric gain of cone**
2 **photoreceptors underpins discrimination of visual scenes**
3 **based on their skewness.**

4 Matthew Yedutenko¹, Marcus H.C. Howlett¹, and Maarten Kamermans^{1,2}

5 ¹Retinal Signal Processing Lab, Netherlands Institute for Neuroscience, Amsterdam,
6 Netherlands

7 ²Department of Biomedical Physics and Biomedical Optics, Amsterdam University Medical
8 Center, University of Amsterdam, Amsterdam, Netherlands

9

10 Abbreviated Title: Cone responses to skewness

11 Corresponding Author: Maarten Kamermans, m.kamermans@nin.knaw.nl

12 10 Figures

13 1 Table

14 Abstract: 169 words

15 Introduction: 648 words

16 Discussion: 1480 words

17

18

19

20

21

22 **Funding**

23 This work was supported by a ZonMW grant 91215062 (M.K.), a grant from Horizon 2020:

24 “Switchboard” (M.K.), a grant of ODAS (M.K.) and a grant of the Foundation of Friends of

25 the NIN (M.K.).

26 **Abstract**

27 Psychophysical data indicates humans can discriminate visual scenes based on their skewness
28 – the ratio of dark and bright patches within a visual scene. It was also shown that on a
29 phenomenological level this skew discrimination is described by the so-called Blackshot
30 mechanism, which accentuates strong negative contrasts within a scene. Here we demonstrate
31 that the neuronal correlate of the Blackshot mechanism is the asymmetric gain of the cone
32 phototransduction cascade, which is higher for strong negative contrasts than for strong
33 positive contrasts. We recorded from goldfish cone photoreceptors and found that the
34 asymmetry in the phototransduction gain leads to higher amplitude of the responses to
35 negatively than to positively skewed light stimuli. This asymmetry in the amplitude was present
36 in the photocurrent, voltage response and cone synaptic output. Additionally, we found that
37 stimulus skewness leads to a subtle change in photoreceptor kinetics. For negatively skewed
38 stimuli, the cone's impulse response functions peak later than for positively skewed stimulus.
39 However, stimulus skewness does not affect the cone's overall integration time.

40 **Significance statement**

41 Humans can discriminate visual scenes based on skewness – the relative prevalence of bright
42 and dark patches within a scene. Here we show that this discrimination originates in the
43 asymmetric gain function of the retinal cone photoreceptors. This gain is higher for the strong
44 negative (dark patches) than for the strong positive (bright patches) contrasts. Thus, we show
45 that cone photoreceptors do not simply relay visual stimuli to downstream circuitry, but also
46 emphasize specific features of those stimuli.

47 **Introduction**

48 Psychophysical studies show that humans are sensitive to the ratio of negative (intensity lower
49 than the mean) and positive (intensity higher than the mean) patches of contrast in visual scenes
50 (Chubb et al., 1994, 2004; Graham et al., 2016). This ratio is described by the parameter known
51 as skewness. Visual stimuli are called positively skewed if there is a predominance of negative
52 contrasts with some infrequent patches of high positive contrast and are called negatively
53 skewed when the situation is reversed. Figure 1 illustrates one's ability to discriminate visual
54 scenes based on skewness by mimicking an experiment performed by Chubb et al. (1994,
55 2004). The textures were randomly drawn from two distributions equal in every aspect but
56 skewness (Bonin et al., 2006). Yet, one can appreciate the clear difference between negatively
57 skewed images (right upper) and positively skewed images (remaining panels). Chubb et al.
58 (1994, 2004) showed that on a phenomenological level the sensitivity to skewness can be
59 described by the so-called Blackshot mechanism. This Blackshot mechanism does not react to
60 skewness per se, rather its sensitivity to strong negative contrasts is simply much higher than
61 to strong positive contrasts and so it effectively reports the fraction of strong negative contrasts
62 within the scene.

63 What are the neuronal correlates of the Blackshot mechanism? Studies using salamander retinal
64 ganglion cells (RGC) (Tkačik et al., 2014) and cat lateral geniculate nucleus neurons (LGN)
65 (Bonin et al., 2006) did not report any response differences associated with changes in stimulus
66 skewness. Therefore, both studies concluded that the discrimination between skewed stimuli
67 occurs in the visual cortex. On the other hand, it is well-established that the retinal
68 photoreceptor's gain is asymmetric: given an equal input magnitude, the response amplitude to
69 a strong (>0.4 Weber unit) negative contrast step is greater than it is to a strong positive contrast
70 step (Laughlin, 1981; van Hateren, 2005; Endeman and Kamermans, 2010; Baden et al., 2013;
71 Angueyra et al., 2021). Furthermore, this responses asymmetry is observed throughout the

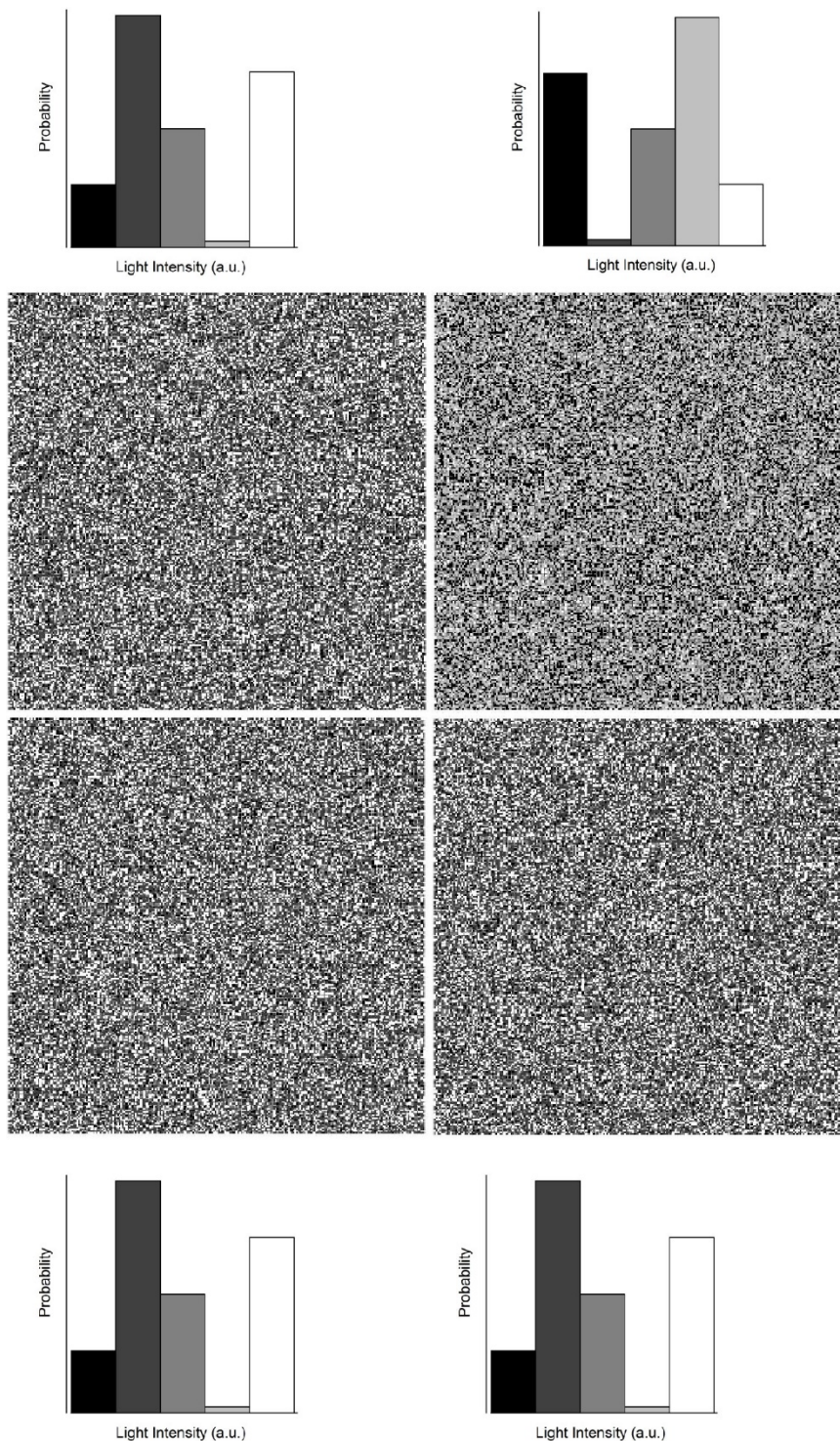


Figure 1

The discrimination of skewed stimuli. An example of textures used by Chubb et al. (1994, 2004) to psychophysically probe the ability of humans to discriminate visual scenes based on their skewness. The textures were randomly drawn from the probability distributions adjacent to each panel following the approach described by Bonin et al. (2006) and differed only in terms of skewness. The upper right texture is negatively skewed (-0.4), the remainder are positively skewed (+0.4).

78 post-receptor retinal stages (Lee et al., 2003; Zaghoul et al., 2003), the LGN (Kremkow et al.,
79 2014), and the primary visual cortex (Zemon et al., 1988; Jin et al., 2008; Yeh et al., 2009;
80 Kremkow et al., 2014). The asymmetrical processing of positive and negative contrasts should
81 lead to different response amplitudes to negatively and positively skewed stimuli and thus
82 might underpin the discrimination of skewed stimuli.

83 A possible reason why the differences in responses to skewed stimuli were not found in RGC
84 (Tkačik et al., 2014) and LGN (Bonin et al., 2006) studies was the power spectra of the stimuli
85 used. In both cases, the researchers employed band-limited white noise, where large
86 proportions of the signal power are outside the photoreceptor frequency bandwidth. Thus, in
87 both studies temporal filtering discarded a significant portion of the signal, reducing the
88 skewness and amplitude of the “effective” light stimuli actually available to photoreceptors.
89 Consequently, Bonin et al. (2006) and Tkacik et al. (2014) may not have found significant
90 differences in the processing of skewed stimuli because a) their stimuli hardly differed in terms
91 of “effective” skewness and b) the “effective” amplitudes of the employed stimuli were too
92 low to drive cone photoreceptors outside their linear response range.

93 Here we address whether photoreceptors process positive and negative skewed stimuli
94 differently. To account for the kinetics of cone photoreceptors, we stimulated goldfish cones
95 with sets of skewed stimuli with bandwidth similar to those of the goldfish cones. We found
96 the asymmetry in goldfish photoreceptor-gain does indeed entail skew-dependent changes in
97 the cone response, leading to greater response amplitudes to negatively than to positively
98 skewed stimuli. This asymmetry originates in the cone phototransduction cascade and is the
99 basis of the Blackshot mechanism. Additionally, we found that the cone’s impulse response
100 function peaks ≈ 3.6 ms later for negatively skewed stimuli whereas the cone’s integration time
101 is unaffected by stimulus skewness.

102 **Materials and Methods**

103 **Recording procedures**

104 All animal experiments were conducted under the responsibility of the ethical committee of
105 the Royal Netherlands Academy of Arts and Sciences (KNAW), acting in accordance with the

106 European Communities Council Directive of 22 July 2003 (2003/65/CE) under license number
107 AVD-801002016517, issued by the Central Comity Animal Experiments of the Netherlands.
108 In all experiments retinas of adult goldfish (*Carassius auratus*) were used.

109 Goldfish were first dark-adapted for 5-10 minutes, sacrificed and the eyes enucleated. Retinas
110 were isolated under dim red illumination then placed photoreceptor side up in a recording
111 chamber (300 μ l, model RC-26G, Warner Instruments) mounted on a Nikon Eclipse 600FN
112 microscope. The preparation was viewed on an LCD monitor by means of a 60 \times water-
113 immersion objective (N.A. 1.0, Nikon), a CCD camera, and infrared ($\lambda > 800$ nm; Kodak
114 wratten filter 87c, United States) differential interference contrast optics. Tissue was
115 continuously superfused with oxygenated Ringer's solution at room temperature (20 $^{\circ}$ C). The
116 composition of Ringer's solution was (in mM): 102.0 NaCl, 2.6 KCl, 1.0 MgCl₂, 1.0 CaCl₂,
117 28.0 NaHCO₃, 5.0 glucose continuously gassed with 2.5% CO₂ and 97.5% O₂ to yield a pH of
118 7.8 (osmolarity 245–255 mOsm). For calcium current (I_{Ca}) measurements, 5 mM of NaCl was
119 substituted with 5mM of CsCl and 100 μ M of niflumic acid added.

120 Measurements from goldfish cones were performed in current- (voltage response), and voltage-
121 (photocurrent), clamp configurations. Patch pipettes (resistance 7-8 MOhm, PG-150T-10;
122 Harvard Apparatus, Holliston, Massachusetts) were pulled with a Brown Flaming Puller
123 (Model P-87; Sutter Instruments Company). Patch pipette solution contained (in mM): 96 K-
124 gluconate, 10 KCl, 1 MgCl₂, 0.1 CaCl₂, 5 EGTA, 5 HEPES, 5 ATP-K₂, 1 GTP-Na₃, 0.1
125 cGMP-Na, 20 phosphocreatine-Na₂, and 50 units ml⁻¹ creatine phosphokinase, adjusted with
126 KOH to pH 7.27–7.3 (osmolarity 265–275 mOsm). The chloride equilibrium potential (E_{Cl})
127 was -55mV except when the calcium current (I_{Ca}) was studied. Here E_{Cl} was set at -41 mV by
128 changing the concentrations of K-gluconate and KCl to 87 and 19 mM, respectively. All
129 chemicals were supplied by Sigma-Aldrich (Zwijndrecht, the Netherlands), except for NaCl
130 (Merck Millipore, Amsterdam, the Netherlands).

131 Filled patch pipettes were mounted on a MP-85 Huxley/Wall-type manual micromanipulator
132 (Sutter Instrument Company) and connected to a HEKA EPC-10 Dual Patch Clamp amplifier
133 (HEKA Elektronik GmbH, Lambrecht, Germany). After obtaining a whole cell configuration,
134 cones were first spectrally classified then stimulated with a set of skewed stimuli of
135 corresponding chromaticity. Data were recorded at a sample rate of 1 kHz using Patchmaster
136 software package (HEKA Elektronik GmbH). In total, we recorded 14 cones in voltage-clamp
137 mode (8 light responses, 6 measurements of I_{Ca}) and 16 cones in current-clamp mode (all light
138 responses). The liquid junction potential (approximately -15 to -16 mV) was not compensated.

139 **Light stimuli**

140 The light stimulator was a custom-built LED stimulator with a three-wavelength high-intensity
141 LED (Atlas, Lamina Ceramics, Westhampton, New Jersey, US). The peak wavelengths were
142 465, 525 and 624 nm. Bandwidth was smaller than 25 nm. Linearity was ensured by an optical
143 feedback loop. The output of the LED stimulator was coupled to the microscope via an optic
144 fiber and focused on cone outer segments through a 60× water-immersion objective. The mean
145 light intensity of all stimuli was 1.2×10^4 photons/ $\mu\text{m}^2/\text{s}$, which is in the photopic level for
146 goldfish (Malchow and Yazulla, 1986). Stimuli were presented at 1 kHz.

147 *Skew Stimulus Set#1*. Skewed stimuli were based on the natural time series of chromatic
148 intensities (NTSCI) from the Van Hateren library (Van Hateren et al., 2002). The NTSCI power
149 spectra is typical of that of ‘natural stimuli’ in that power declines as a function of
150 frequency (Van Hateren, 1997; Van Hateren et al., 2002; Frazor and Geisler, 2006). As a result
151 of the predominance of lower frequencies, most of the light intensity changes throughout the
152 NTSCI occur over timescales accessible to goldfish cones and previously the NTSCI has been
153 used to unlock several non-linear performance features of cones (Endeman and Kamermans,
154 2010; Howlett et al., 2017). To ensure that all aspects other than skewness remained equal, we

155 first picked short stretches from the NTSCI that were positively skewed, then simply flipped
156 these around the mean to generate negatively skewed stimuli.

157 To generate Stimulus set#1 we divided the NTSCI (Van Hateren et al., 2002) into one-second
158 long stretches. Then from each stretch we subtracted its minimum value, adjusted their mean
159 light intensities to be equal and picked stretches with similar power spectra and root mean
160 square (r.m.s.), and median contrasts (between 0.23 and 0.25). The r.m.s. and median contrast
161 for each stretch was calculated respectively as the ratio between the stretch's standard deviation
162 and its mean, and the ratio between its deviation from the median, and its median. To ensure
163 an absolute similarity between positively and negatively skewed stimuli, we selected only
164 stretches where the maximum value was not larger than 2 times the mean. Next, we chose
165 stretches with skewness's of 0.9, 1.6, 2.2. The skewness was calculated with the equation (1):

$$166 \quad S = \left\langle \frac{(I - I_{\text{mean}})^3}{N\sigma^3} \right\rangle \quad (1)$$

167 where N is the number of elements in stretch, I correspond to the light intensity of an element,
168 I_{mean} and σ are mean and standard deviation within the stretch and brackets denotes averaging
169 over the period.

170 We further narrowed our selection to three stretches all with similar power spectra (data not
171 shown). Power spectra were calculated by Welch's averaged periodogram method (Welch,
172 1967). No window function was used, the length of the Fourier transform was same as the
173 length of each corresponding data sequence. Total stimulus power was calculated as the
174 integral under power spectra, the differences in the total stimulus power were no more than
175 10%. Finally, an additional pink noise stimulus with zero-skew and similar power spectra was
176 added to the set. In total, Skew Stimulus set#1 consisted of seven 1-second stimuli.

177 *Skew Stimulus set#2*. This stimulus set consisted of three 4-second long stretches with a
178 skewness of 2.2, 0, and -2.2. They were generated in the same way as the Skew Stimulus set#1,
179 but with one additional condition: the degree of skewness delivered by the stimulus remained
180 unchanged by the cone's temporal filtering. This was ensured by first convolving the NTSCI
181 stretch with the mean photocurrent impulse response function (see below) obtained from
182 responses to Skew Stimulus set #1. The skew of the convolution product, representing the
183 "effective" stimulus, was then compared with the skew of the original stimulus (Figure 3). This
184 was further confirmed by determining the effective skewness after convolving the stimuli with
185 the impulse response function of each cone measured under Skew Stimulus set #2 conditions
186 (Figure 3B).

187 **Calcium current isolation**

188 To measure I_{Ca} , we used the mean voltage response (7 cells, 69 repeats in total) of cone
189 photoreceptors to Stimulus set #2 as the command voltages for the voltage clamp experiments.
190 To isolate I_{Ca} we followed the approach described by Fahrenhofs et al. (Fahrenfort et al., 1999).
191 Briefly, to eliminate the calcium-dependent chloride current E_{Cl} was set at -41 mV and 100 μ M
192 of niflumic acid added to the Ringer's solution; delayed rectifying, and hyperpolarization-
193 activated, potassium currents were blocked by substituting 5 mM of NaCl in Ringer's solution
194 with 5 mM of CsCl; light-activated conductances were saturated by a 20 μ m spot of bright
195 white light focused on the cone outer segment; linear leak currents were removed by
196 subtraction. The leak current was estimated by clamping cones at -70mV, stepping to potentials
197 between -100 and 20 mV in 5 mV steps for 100 ms, calculating the mean current between 20
198 and 60 ms after the step onset, then determining the linear fit of the IV-relation between -100
199 and -60 mV (Vroman et al., 2014; Kamar et al., 2019).

200 **Data analysis**

201 For each cell, the skewness of its mean response to each stimulus was determined using
202 equation (1). In Figures 2, 3D and 8A, data was fitted using build-in Matlab least square
203 methods. All data analysis was performed in Matlab and Python.

204 Parallel cascade identification is the most rigorous method to describe the signal processing
205 properties of cone responses to naturalistic stimuli (Korenberg, 1991) . However, for practical
206 reasons our analysis only focuses on the estimation of the first parallel cascade, which is
207 effectively a linear filter followed by a static non-linearity. Apart from the computational and
208 descriptive simplicity, this approach is also justifiable as it accurately describes cone responses,
209 accounting for over 95% of the variance (Figure 8A).

210 The linear temporal filtering properties of a cone was described by its impulse response
211 function. Impulse response functions were estimated as the inverse Fourier transform of the
212 ratio between stimulus-response cross-power and stimulus power spectrum (Wiener, 1964;
213 Kim and Rieke, 2001). The spectra were calculated using Welch averaged periodogram method
214 (Welch, 1967). Stimuli and responses were detrended, divided into 500 ms long stretches, with
215 50% overlap, and windowed with a hamming function. The length of the Fourier transform
216 was 1024 ms. Cone integration time was calculated as the integral of the impulse response
217 function's initial polarization lobe (Daly and Normann, 1985).

218 To estimate the effective” stimuli perceived by each cone photoreceptors during each stimulus,
219 we convolved the cone's impulse response function during that condition with the original light
220 stimulus. Skews of these “effective” stimuli were calculated with equation (1). Discrepancies
221 between the skewness of the “effective” stimuli and the skewness of the cone's responses, were
222 considered a result of non-linear cone properties.

223 For “effective” Weber contrast steps (Figures 7&8A), light stimuli were first converted into
224 Weber contrasts steps (Figure 7) with equation (2):

$$225 \quad C = \frac{(I - I_{mean})}{I_{mean}} \quad (2)$$

226 These Weber contrast steps were then convolved with a mean impulse response function to
227 obtain the “effective” Weber contrast steps. The mean impulse response function used here
228 was the averaged voltage-response derived impulse response function of all 16 cones measured
229 in current clamp, which was subsequently scaled such that the integral under its curve yielded
230 one (Figure 7; Howlett et al., 2017). Even though a cone’s impulse response function is affected
231 by the skewness of the stimulus (Figure 8B&C), we used this mean impulse response function
232 for the following reasons.

233 Firstly, observed changes to the impulse response function shape had little effect on the cone
234 response dynamics. We convolved Skew Stimulus Set #2 with impulse response functions
235 derived from responses to positive and negative stimulus of each of the cones (n=7) and found
236 that the resulting convolution products were highly correlated ($r \approx 0.98 \pm 0.01$). Secondly,
237 averaging across different stimulus skew conditions was crucial to account for biases in the
238 estimate of the amplitude of the impulse response function arising from skewness of the light
239 stimuli (Chichilnisky, 2001; Simoncelli et al., 2004; Bonin et al., 2006; Tkačik et al., 2014).
240 Finally, the goal of this analysis was to illustrate cone photoreceptor gain asymmetries rather
241 than to provide a veridical description of the gain dependence on stimulus contrast.

242 To estimate the cone’s non-linear gain function parameters we fitted the relationship between
243 all the mean cone voltage responses and the “effective” Weber contrast steps (Figure 8A, 19000
244 data points) as the power function of input contrast (Van Hateren and Snippe, 2006) with
245 equation 3:

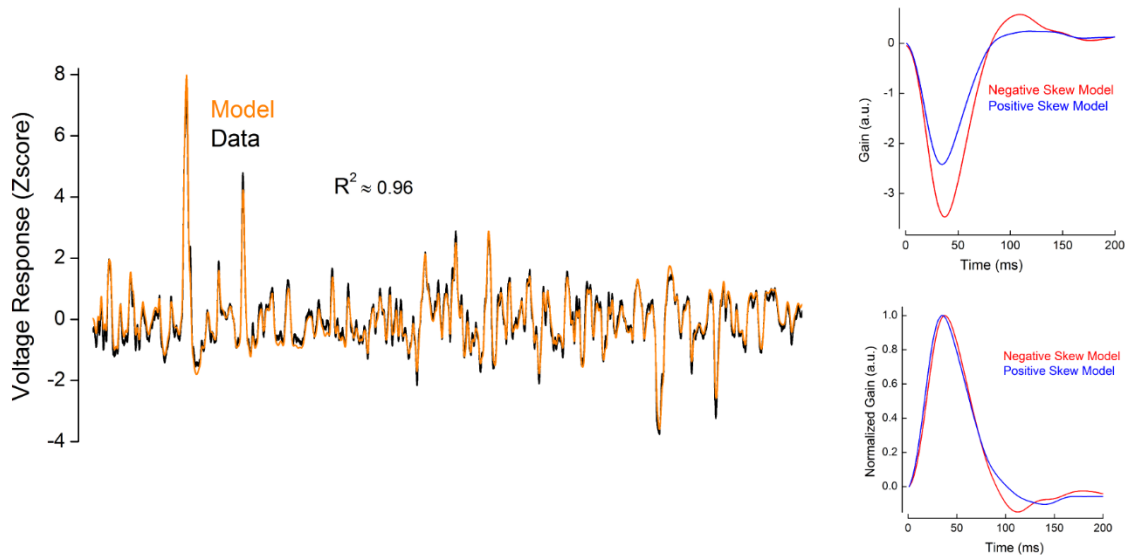
246
$$\Delta V = a * (C + b)^d + e \quad (3)$$

247 Here ΔV denotes voltage response, C is the “effective” Weber contrast, a, b, d, and e are fit
248 parameters. At the biophysical level b) corresponds to the baseline rate of phosphodiesterase
249 activity (PDE), d) describes the inter-dependence between the PDE activity rate and the voltage
250 response, e) is proportional to the baseline concentration of cyclic guanosine monophosphate
251 and a) is a scaling factor (Van Hateren and Snippe, 2006). The quality of the fit was quantified
252 with the adjusted coefficient of determination (R^2). The highest R^2 (0.95) was obtained using
253 the following parameter values (value \pm 95 % confidence interval): a=0.05138 \pm 0.03506,
254 b=1.166 \pm 0.072, d= -0.1251 \pm 0.0959, e=-0.05046 \pm 0.03552. Our estimation of the power
255 function (d) was close to that obtained by Van Hateren and Snippe (2006) in their theoretical
256 study.

257 **Model**

258 Photoreceptor responses were modelled in matlab using Van Hateren’s model of vertebrate
259 photoreceptors (van Hateren and Snippe, 2007), which was shown to be remarkably precise in
260 capturing the processing steps involved in generating a cone’s signal. Apart from the activation
261 of hyperpolarization-activated current (I_h ; Howlett et al., 2017; Kamermans et al., 2017), the
262 model closely simulates all the cone’s biophysical processing steps from the photon-initiated
263 activation of conopsins to the cGMP-regulated changes in the photocurrent, followed by the
264 generation of the voltage response. The model simulates cone photoreceptors as a cascade of
265 low-pass filters, a static (instantaneous and memoryless) non-linearity, and two divisive
266 feedback loops (van Hateren, 2005; van Hateren and Snippe, 2007). The low-pass filters
267 correspond to the kinetics of the different biophysical processing steps. The non-linearity
268 describes the inverse proportional dependence between light intensity and changes in the
269 cGMP concentration. The first feedback loop describes the regulation of the rate of cGMP

270 production by calcium influx through cGMP-gated channels. The second feedback loop
271 corresponds to the regulation of the membrane voltage by voltage-sensitive channels in the
272 cone inner segment. The cone's non-linear gain (Figure 8A) originates from the interplay
273 between the hydrolysis of the cGMP by PDE and calcium-regulated (feedback loop) production
274 of the cGMP by guanylyl cyclase (GC)



275

276 **Figure 2**

277 Example of the performance of the Van Hateren model for goldfish cones. Left. Voltage responses as Z-scores to
278 Skew Stimulus set #2 for a representative recorded cone (black line) and for the simulated cone (orange line). The
279 coefficient of determination (R^2) between these two traces was 0.98. Right. Impulse response functions obtained
280 from the simulated responses to negatively (red) and positively (blue) skewed stimuli. Parameters for the
281 simulation are listed in the Table 1.

282 We verified that the Van Hateren model could capture responses to skewed stimuli. For this
283 we fitted the model to the voltage responses of 7 goldfish cones recorded under Skew Stimulus
284 Set#2 conditions. The model parameters were modulated within the ranges determined by
285 Endeman and Kamermans (2010) and are shown in the Table 1. For all 7 cells, the correlation
286 coefficient between modelled and recorded voltage responses were no less than 0.97 (adjusted
287 $R^2 \geq 0.94$ Figure 2). Moreover, the impulse response functions estimated from the simulated

288 responses to positively and negatively skewed stimuli retained features of the impulse response
289 functions derived from the recorded voltage responses. For example, for both recorded and
290 simulated cone voltage responses, impulse response functions peaked 3 ms ($8.5 \pm 1\%$,
291 $p=0.00013$) later under the negatively skewed stimulus compared to the positively skewed
292 condition but showed no statistically significant difference in their full width at half maximum
293 (FWHM), or in integration time (Figure 2). Thus, Van Hateren's model reproduces accurately
294 cone responses to skewed stimuli.

295 Next, we used the Van Hateren model to estimate the "effective" stimuli perceived by
296 salamander and cat cones in the studies by Tkacik et al. (2014) and Bonin et al. (2006),
297 respectively. To model salamander cones we adjusted the parameters of Van Hateren's model
298 such that the time course of the impulse response functions of simulated cones resembled those
299 of salamander cones reported by Rieke (2001) and Baccus and Meister (2002). The exact
300 simulation parameters are reported in the Table 1. Similarly, to model cat cones the Van
301 Hateren model parameters were adjusted so that the impulse response function time course
302 resembled the estimates made by Donner and Hemila (1996). For the cat, exact parameters of
303 the simulation are reported in the Table 1.

304 "Light" stimuli mimicking those used by Bonin et al. and Tkacik et al. (2014) where
305 respectively used to study the responses of the modelled cat (Figure 9) and salamander (Figure
306 10) cones to changes in skewness. The only difference was that for illustrative ease the
307 positively and negatively skewed stimuli were mirror copies of each other. Cat stimuli had a
308 r.m.s. contrast of 0.7, skews of ± 0.4 and a flat power spectrum bandlimited to 124 Hz.
309 Salamander stimuli had a r.m.s. contrast of 0.2, skews of ± 2 and a flat power spectrum
310 bandlimited to 30 Hz.

311 **Statistics**

312 All data are presented as mean \pm SEM unless otherwise stated. Differences between groups
313 were tested using two-tailed t-test (Student, 1908).

314 **Results**

315 **Cone responses vary with skewness**

316 To assess the photoreceptor's contribution to skew discrimination, we exposed goldfish cones
317 to a series of modified naturalistic time series of chromatic intensities (NTSCI) from the Van
318 Hateren library (Van Hateren et al., 2002; Skew Stimulus set#1 in Material and Methods) and
319 recorded their photocurrent and voltage responses (Figure 3A). Stimuli were equal in terms of
320 mean intensity, root mean square contrast and median contrast, and had similar power spectra,
321 while their skewness varied from -2.2 to +2.2. Positively and negatively skewed stimuli were
322 mirror copies of each other, therefore any asymmetries between corresponding responses
323 would reflect an asymmetry in the cone's processing.

324 To determine whether cones process negatively and positively skewed light stimuli differently,
325 we plotted the skews of the photocurrent (Figure 3B) and voltage responses (Figure 3C) against
326 the skews of the light stimuli. If there is no difference in processing, the skewness of the
327 response will be equal to the light stimulus skewness and thus the data points will fall along a
328 straight slope. However, if there is an asymmetry in the processing of positive and negative
329 contrasts it would necessarily lead to the deviation of the data points from the grey line. Figures
330 3B&C shows that for positively skewed stimuli, the photocurrent and voltage responses are
331 skewed to a lesser degree than are the light stimuli, whereas for the negatively skewed stimuli
332 they are almost as equally skewed as the light stimuli. Note that the signal sign-inversion of
333 the voltage response also sign-inverts its skewness. Figures 3B&C indicate an asymmetry in
334 the processing of negatively and positively skewed stimuli by cone photoreceptors.

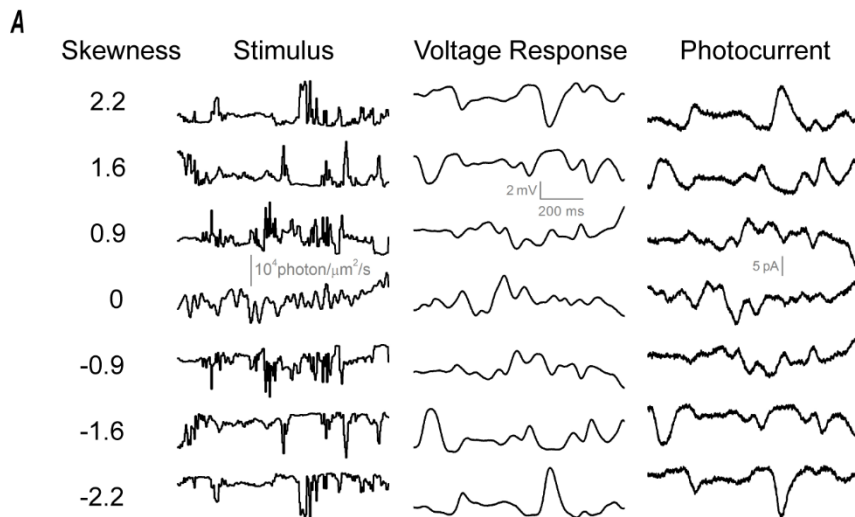
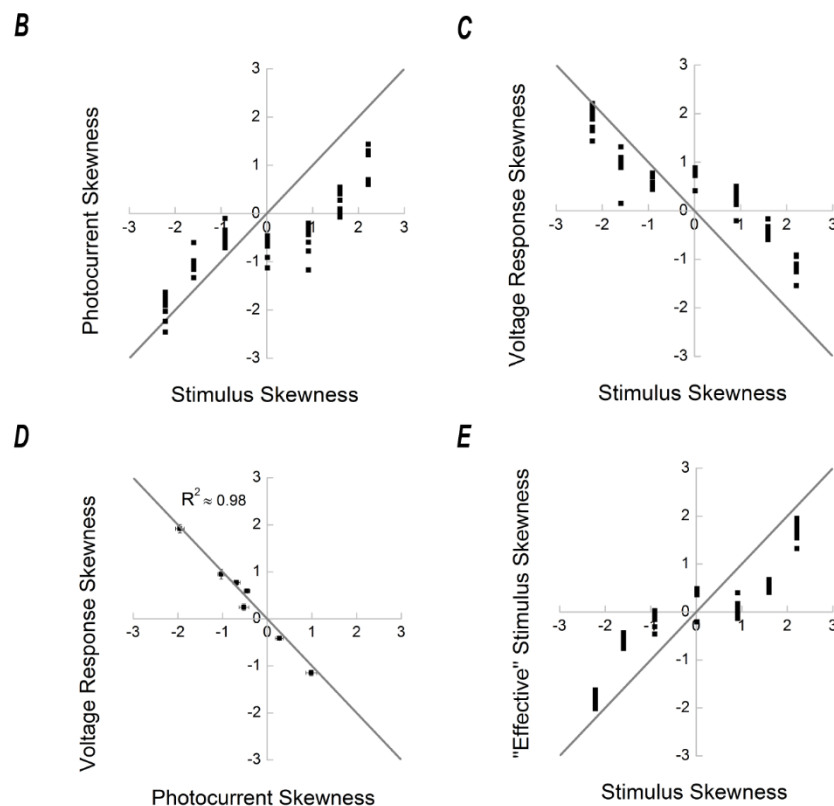


Figure 3

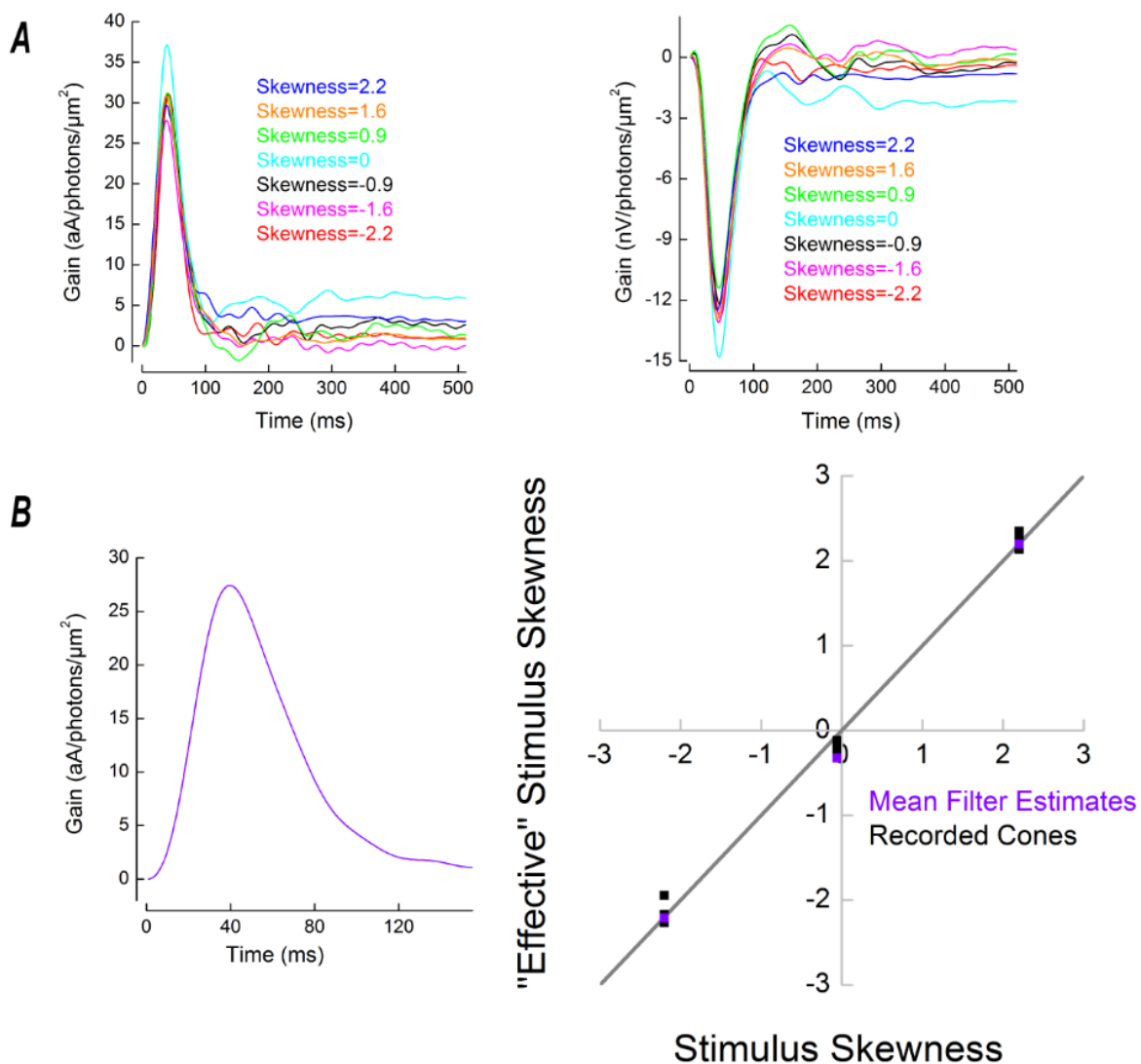
Cone processing affects stimulus skewness. **A.** Skew Stimulus set#1 (left) together with examples of voltage (middle), and photocurrent (right), responses recorded from cone photoreceptors. **B.** Photocurrent skewness as a function of stimulus skewness for Skew Stimulus set #1 (n=8). Each black square represents the skewness of a cell's photocurrent response to a skewed stimulus condition. The grey line depicts the situation where the response skewness is equal to the stimulus skewness. The panel shows cone responses to positive skewed stimuli were less skewed than their



357 stimulus, but to stimuli with zero or negative skews cone responses were more skewed than their stimulus. **C.**
 358 Voltage response skewness as a function of stimulus skewness (n=9). Note that the voltage responses and stimuli
 359 skews have different sign due to the signal sign-inversion. The grey line describes the situation where response
 360 and stimulus skews are equal in magnitude. As was the case in B), cone responses to positive skewed stimuli were
 361 less skewed than their stimulus. To stimuli with zero or negative skews, the skewness of the cone's response was
 362 greater than that of its stimulus. **D.** Skewness of the voltage response as a function of the photocurrent. For each
 363 stimuli condition, the skews of each corresponding voltage response, and photocurrent, were averaged and the
 364 resulting means (\pm SEM) plotted as a voltage response verses photocurrent function. Note that as the cone's voltage

365 response is sign-inverted relative to its photocurrent their skews are also sign inverted. The situation where the
 366 voltage response and photocurrent have equal magnitude of skewness is described by the grey line, which fits the
 367 data with adjusted R^2 of ≈ 0.98 . This indicates that the asymmetric processing of positively and negatively skewed
 368 inputs originates in the phototransduction cascade. **E.** “Effective” skewness perceived by the cones as the function
 369 of the skewness of the light stimuli. “Effective” skews were estimated from the convolution product of the light
 370 stimuli with the cone’s impulse response function (Figures 4A&B). The grey line depicts the situation, where
 371 “effective” and response skews are equal. Note that for illustrative convenience the “effective” skewness
 372 estimated from voltage responses were multiplied by -1. Figure 3E indicates that even though naturalistic stimuli
 373 were used, some aspects of the stimuli were still unavailable to drive cone responses on account of the cone’s
 374 temporal filtering properties. This in turn reduced the range of “effective” skews by almost 30% relative to the
 375 original -2.2 to +2.2 range of stimulus skews.

376



377 **Figure 4**

378 **A.** Representative examples of the cone impulse response functions obtained using the photocurrent (left) and
379 voltage responses (right) to Skew Stimulus set #1. **B.** Left. The mean cone impulse response function obtained as
380 the averaged photocurrent impulse response functions to all of the stimuli in Skew stimulus set#1 in all of the
381 recorded cells (n=8) (Figure 4A left). This mean photocurrent impulse response function was used, via
382 convolution, to identify segments of the NTSCI where the skewness of the original and “effective” stimuli
383 remained equal, a subsection of which formed Skew stimulus set#2. Right. Skewness of the “effective” stimuli as
384 a function of the skewness of the original stimuli for Skew Stimulus set #2. Violet squares correspond to the
385 “effective” skewness obtained by the convolution of the light stimuli with the mean impulse response function
386 shown on the left. Black squares depict the “effective” skewness ‘perceived by each cone under Skew Stimulus
387 set #2 conditions. This was estimated by convolving each Skew Stimulus set #2 stimulus with the cone’s impulse
388 response function obtained for corresponding stimulus. The grey line describes the condition where temporal
389 filtering does not affect stimulus skewness. Since all squares are aligned with the grey line, the “effective”
390 skewness is approximately equal to the original light stimulus skewness. Hence, for Skew Stimulus set #2 cone
391 temporal filtering does not change the skewness delivered by the stimuli.

392

393 **The processing asymmetry originates exclusively within the**
394 **phototransduction cascade**

395 What are the cellular mechanisms leading to the differences in the processing of negatively and
396 positively skewed stimuli? To tease apart the relative contributions of the phototransduction
397 cascade and the voltage activated membrane conductances, we plotted the skewness of the
398 voltage responses and photocurrent against each other in Figure 3D. The grey line depicts the
399 condition where photocurrent and voltage response skews are equal in magnitude. All data
400 points fall on this line ($R^2=0.98$), meaning that the skewness of the photocurrent accounts for
401 98% of the skewness of the voltage responses. This means that the phototransduction cascade
402 is the primary source of the asymmetric processing of the positively and negatively skewed
403 stimuli.

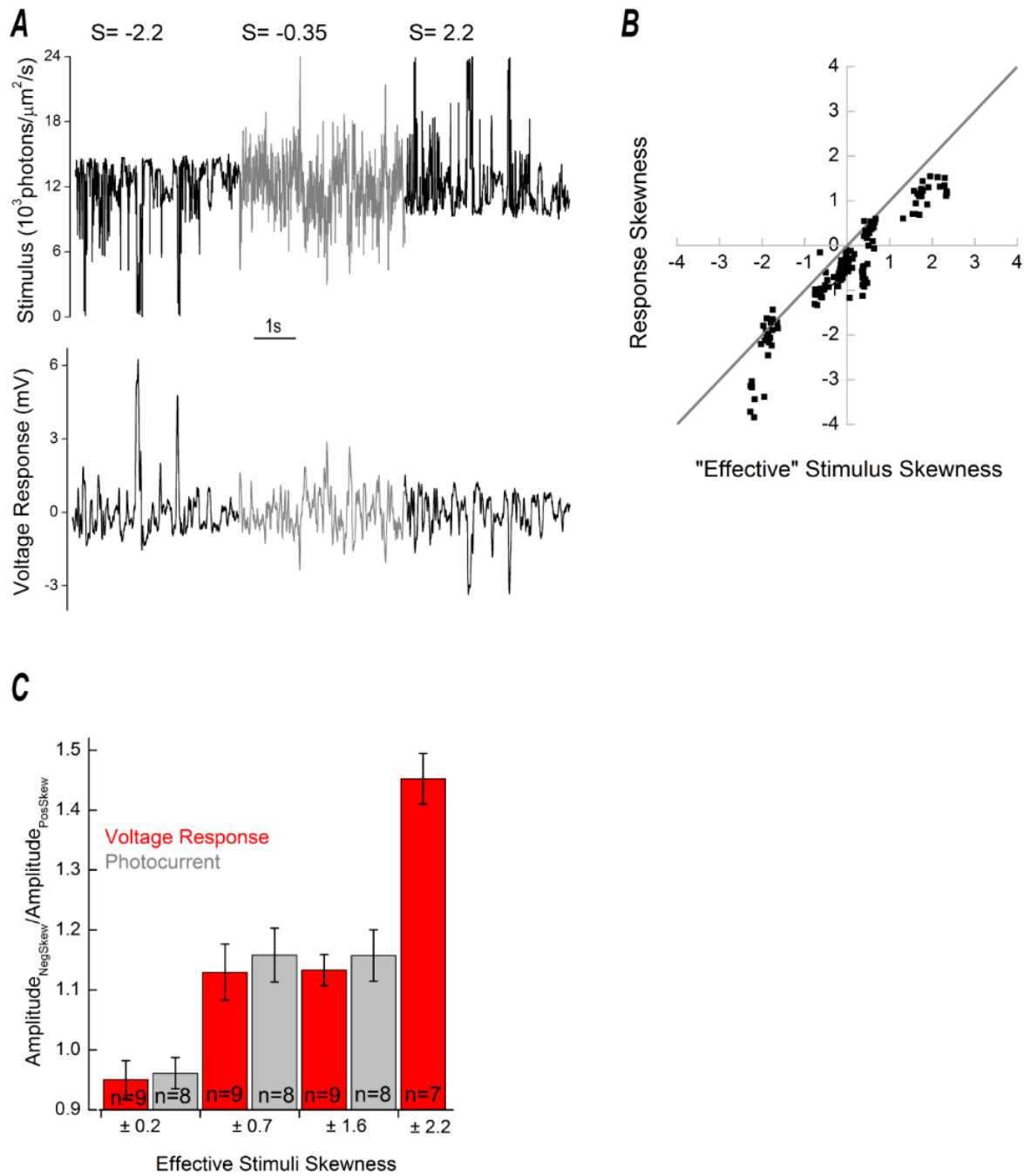
404 **Temporal filtering affects stimulus skewness**

405 A cone's finite kinetics may act to temporally filter our light stimulus and thus affect the
406 skewness of the "effective" stimulus perceived by a cone. To determine the "effective" stimuli
407 skews we first estimated the temporal filters of the cone's photocurrent responses to each of
408 the skewed stimuli stretches following the Wiener approach (Wiener, 1964; Rieke, 2001;
409 Figures 4A&B). Next, we convolved the estimated filters with their corresponding skewed
410 stimuli to obtain the "effective" stimuli perceived by cone photoreceptors. Then we calculated
411 the skews of the "effective" stimuli and plotted them against the skews of the original light
412 stimuli on the Figure 3E, where the grey line describes the situation where the "effective" skew
413 is equal to the original skew. Data points for the positively skewed light stimuli are lower than
414 the grey line and higher for the negatively skewed light stimuli. Consequently, temporal
415 filtering reduced the "effective" skewness perceived by the cones.

416 **Asymmetry in the responses to "effective" stimuli**

417 How do goldfish cones process these "effective" stimuli? Figure 3E shows that linear temporal
418 filtering reduces "effective" skewness and decreases the dynamic range over which responses
419 to skewed stimuli were measured by almost 30% (from ± 2.2 to ± 1.6). Therefore, we first
420 completed our data set by recording the cone's voltage responses to stimuli with "effective"
421 skews of ± 2.2 (Figures 4C&5A). Next, we plotted the skews of the responses against the
422 "effective" stimulus skews (Figure 5B) and found that goldfish cones decrease the magnitude
423 of skewness when the stimuli are skewed positively and increase the magnitude of skewness
424 when the stimuli are skewed negatively.

425 Asymmetry in the processing of negatively and positively skewed stimuli is also reflected in
426 the amplitudes of the corresponding responses: standard deviations of the responses to
427 negatively skewed stimuli were up to 50% larger than the standard deviations of the responses
428 to positively skewed stimuli (Figure 5C).



429 **Figure 5**

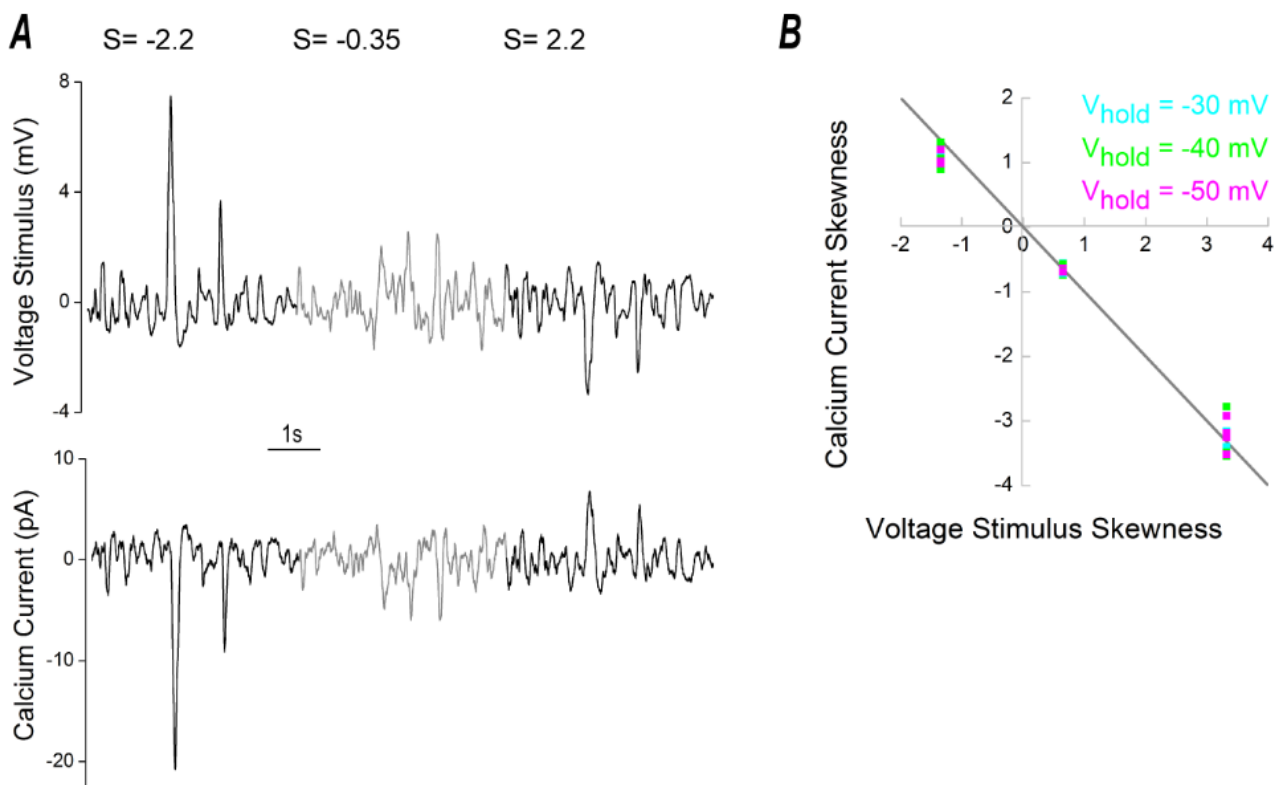
430 Asymmetries in cone responses to positively and negatively skewed stimuli. **A.** Top. Depiction of Skew Stimulus
 431 set #2. The key property of this stimulus set is that the light stimulus skewness is not affected by the temporal
 432 filtering properties of cones (Figure 3B). Bottom. An example of a recorded voltage response to Skew Stimulus
 433 set #2. **B.** Skews voltage and photocurrent responses against the “effective” stimuli skews. This figure illustrates
 434 the relation between “effective” stimulus skew (see Figure 3E, Figure 4B) and the skewness for the photocurrent
 435 ($n=8$) and voltage responses ($n=9$) of cones stimulated with Skew Stimulus set #1, and the voltage responses of
 436 cones ($n=7$) recorded with Skew Stimulus set #2. This data indicates the cone response skewness differ from the

437 skewness of the “effective” stimulus. Cone responses are less skewed than the stimulus when it delivers higher
438 levels of positive “effective” skew. The opposite occurs when the stimulus delivers higher levels of negative
439 “effective” skew, the cone responses are more skewed than the stimulus. The grey line depicts the situation where
440 the cone response and “effective” stimulus are equally skewed. For illustrative convenience, the voltage responses
441 skews were multiplied by -1. C. Differences in cone response amplitudes (photocurrent – grey, voltage response
442 – red) to negatively and positively skewed stimuli for each “effective” skew stimuli pair. When the “effective”
443 skew magnitude was low (± 0.2) the photocurrent or voltage responses amplitudes were unaffected by the skew
444 direction. However, at higher “effective” skew-magnitudes cone response amplitudes to negatively skewed stimuli
445 were larger than for positively skewed stimuli (photocurrent difference: ± 0.7 , $15.8\% \pm 4.52\%$ $p=0.01$; ± 1.6 , 15.7
446 $\pm 4.33\%$ $p=0.0083$; voltage response difference: ± 0.7 , $13.0 \pm 4.67\%$ $p=0.024$; ± 1.6 , $13.3 \pm 2.64\%$ $p=0.00097$;
447 ± 2.2 , $45.2 \pm 4.20\%$ $p=0.00004$). Changes in response amplitude were assessed as the ratio of standard deviations
448 of a cell’s response to corresponding negatively and positivity skewed stimuli. The “effective” skew values shown
449 were estimated by the mean impulse response (Figure 7), obtained using the impulse response functions of all
450 cells under all stimuli conditions. Data shown as mean \pm SEM.

451

452 **Asymmetry in the cone's output**

453 To be perceived by the downstream neurons, asymmetries in the cone's responses to positively
454 and negatively skewed stimuli (Figures 5B&C) should be reflected in the synaptic release. In
455 photoreceptors, glutamate release is directly proportional to the calcium current (Schmitz and
456 Witkovsky, 1997; Thoreson et al., 2004). Consequently, one can estimate changes in cone
457 glutamate release by recording its calcium current (I_{Ca}).



458

459 **Figure 6**

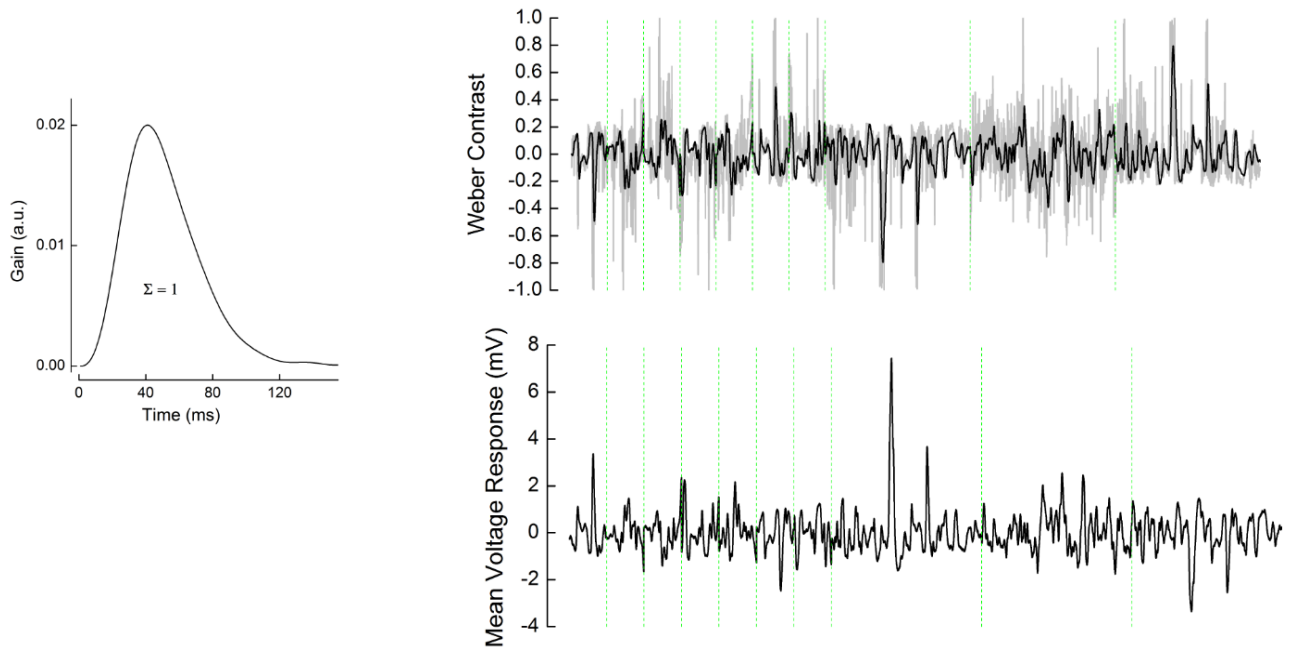
460 Asymmetrical processing of skewed stimuli at the cone I_{Ca} level. **A.** Top panel depicts the mean cone voltage
461 response to Skew Stimulus set #2, which was used as the stimulus for I_{Ca} measurements. An example I_{Ca}
462 measurement, when using this stimulus, is shown in the bottom panel. **B.** Skewness of I_{Ca} as a function of stimulus
463 skewness. The measurements of I_{Ca} were performed at three different potentials along its activation curve: -30mV
464 (cyan), -40mV (green) and -50mV (magenta). Note that as a decrease in voltage causes an increase in I_{Ca} , skews

465 for the stimulus and response have opposite signs. The grey line denotes the situation where I_{Ca} and its stimulus
466 are equally skewed. Regardless of the holding potential, data points are aligned with grey line, indicating that the
467 cone's I_{Ca} maintains any skewness present in its voltage response. Since cone-photoreceptor glutamate-release is
468 directly proportional to I_{Ca} (Schmitz and Witkovsky, 1997; Thoreson et al., 2004), it is highly likely cone output
469 retains any I_{Ca} skewness.

470
471

472 We measured skew-dependent modulation of I_{Ca} by using recorded voltage responses to light
473 stimuli with “effective” skews of ± 2.2 and -0.35 as the command voltages at three different
474 potentials (-30 , -40 , -50 mV) along the I_{Ca} activation curve (Figure 6A). To isolate I_{Ca}
475 responses, we blocked all other active conductance and subtracted the leak current. We then
476 plotted the skews of the I_{Ca} signals against the skews of the voltage responses (Figure 6B).
477 Note, that since depolarization produces an inward I_{Ca} , the skews of the voltage response and
478 I_{Ca} response have opposite signs.

479 Regardless of the clamping potential, all the data points in Figure 6B approximately fall on the
480 grey line, indicating that the skewness of the cone's signal is largely unaffected by the
481 transformation from membrane potential to the I_{Ca} . Consistent with this, the amplitudes of I_{Ca}
482 during the $+2.2$ and -2.2 skew conditions differed to the same degree (from $50 \pm 1.2\%$ to $54 \pm$
483 1% depending on the holding potential) as those of the voltage responses (Figure 5C). Thus,
484 for negatively and positively skewed stimuli, the asymmetries present at the cone's earlier
485 processing stages are preserved and even somewhat enhanced in the cone's output.



486

487 **Figure 7**

488 “Effective” Weber contrast steps. Left. Mean impulse response function used to obtain “effective” Weber contrast.

489 The mean impulse response was estimated by averaging the individual voltage-responses impulse-response

490 functions of all cells for all stimuli ($n=16$) (Figure 4A right, Figure 8B). This mean was scaled such that the

491 integral under its curve was 1. Right. Upper. Grey line: The original light stimuli of Skew Stimulus set #1 and

492 set#2 converted to Weber contrast steps. Black line: The “effective” Weber contrast steps obtained by the

493 convolution of the original Weber contrast steps with the mean impulse response function shown on the left.

494 Bottom. The averaged cone voltage response to each stimuli. For both upper and lower panels, the green dashed

495 lines separate the different stimuli stretches during which the effective skews were (from left to the right): -1.6, -

496 0.2, 0.2, -0.7, 0.06, 1.6, 0.7, -2.2, -0.35, 2.2.

497

498

499 **Asymmetrical gain of the cone photoreceptors**

500 What type of non-linear gain leads to the skew-dependent changes in the amplitude of the cone

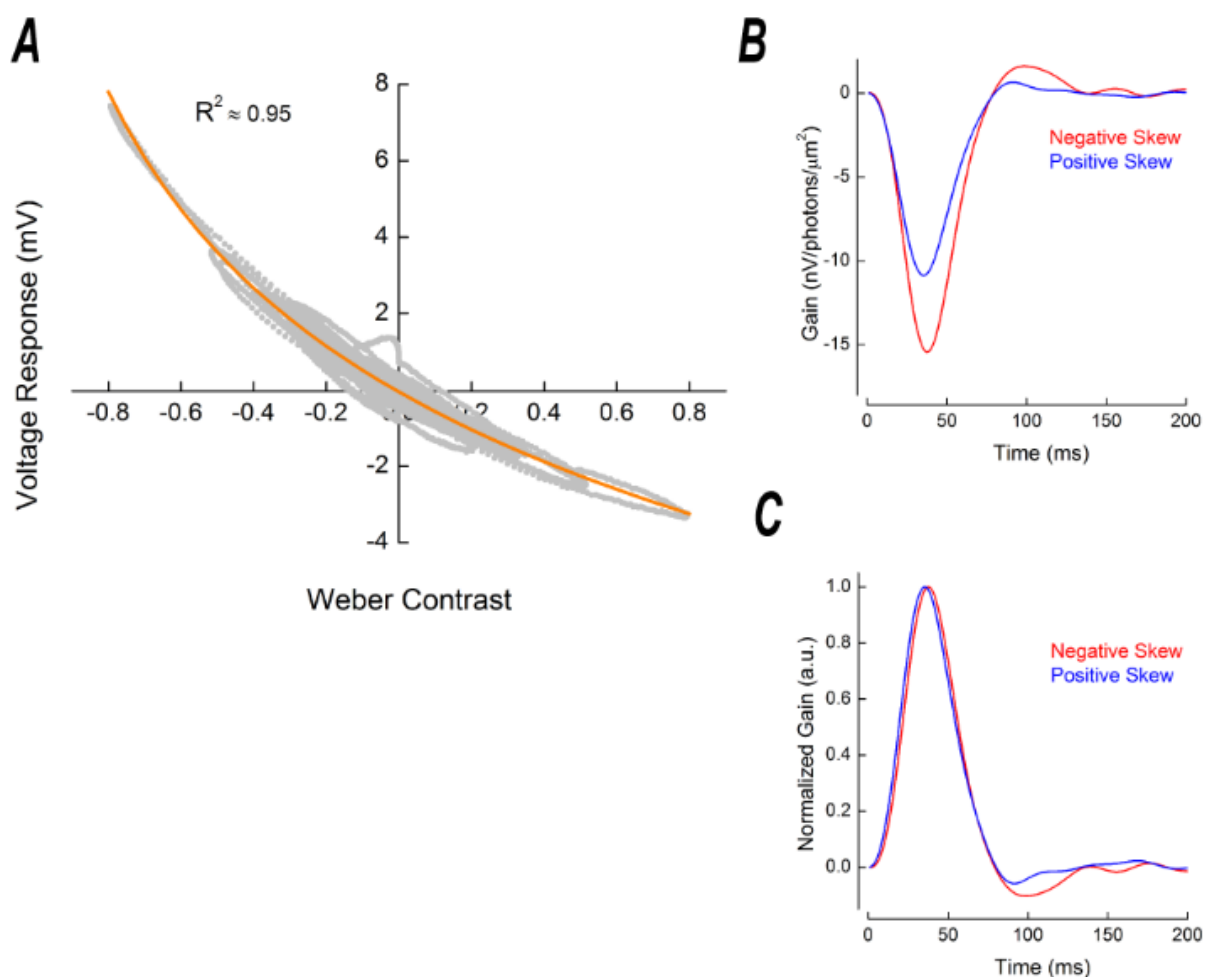
501 responses? To determine how the voltage response amplitude depends on the Weber contrast

502 step we first converted the “effective” stimuli intensities into Weber contrast steps (Figure 7).

503 Next, we plotted baseline subtracted mean voltage responses (Figure 7) as a function of the

504 “effective” Weber contrast steps (Figure 8A). Figure 8A shows that cone responses are larger
505 for Weber contrast steps below -0.4 than they are for Weber contrast steps above 0.4. Hence,
506 the response gain of cones is greater for high negative, than for high positive, contrasts.

507 What kind of input-output relation supports the asymmetric gain of cones? We fitted the
508 relation between voltage responses and “effective” Weber contrast steps with equation (3)
509 (Figure 8A orange) and found that the cone voltage response is proportional to Weber contrast
510 step with an exponent of -0.1251 ($R^2 \approx 0.95$, 95% confidence interval ± 0.0959). This
511 dependence is close to the one determined in the theoretical study by Van Hateren and Snippe
512 (2006), who suggested that voltage responses of the vertebrate cone is proportional to Weber
513 contrast with an exponent of -0.12.



514 **Figure 8**

515 The cone signal transfer properties. **A.** Asymmetric gain of cone photoreceptors. To estimate cone photoreceptor
516 gain, we plotted the voltage response of cones as a function of “effective” Weber contrast. This relationship was
517 well described (orange line, adjusted $R^2 = 0.95$) by the Weber contrast power function given in equation (3) and
518 clearly indicates that cone gain is higher for negative contrasts than for the positive contrasts. The differences
519 become prominent from Weber contrast steps around ± 0.4 and are especially vivid for contrast steps beyond ± 0.6 .
520 “Effective” Weber contrast was obtained by converting the light intensities into Weber contrast steps with
521 equation (2), which were then convoluted with the mean cone impulse response function scaled such that integral
522 under its curve yielded 1 (see methods, Figure 7). The voltage response shown is the baseline-subtracted average
523 of all cells for each stimulus conditions. In total, there are 19000 data points in this figure. **B.** Stimulus skewness
524 changes the shape of the cone’s impulse response function. The figure depicts two representative examples of a
525 cone’s impulse response function in conditions with -2.2 (red) and +2.2 (blue) “effective” stimulus skewness. **C.**
526 The cone impulse response functions shown in **B**, normalized by the amplitude of their initial lobe. On average,
527 impulse response functions peaked 3.6 ms, or $9 \pm 1.0 \%$, later for negatively skewed stimulus than for the
528 positively skewed condition ($p=0.0001$, $n=7$) whereas the impulse response function FWHM ($\Delta = 1 \pm 1.35 \%$,
529 $p=0.37$, $n=7$) and the cone integration time ($\Delta = 1.1 \pm 1.61 \%$, $p = 0.51$, $n=7$) were unchanged.

530

531 **Stimulus skewness affects the shape of the cone impulse response function**

532 The processing time of cones is inversely proportional to light intensity such that responses to
533 steps of strong positive contrast peak earlier than responses to strong negative contrasts
534 (Nikonov et al., 2000; Lee et al., 2003; van Hateren, 2005; Van Hateren and Snippe, 2006;
535 Angueyra et al., 2021). Therefore, one might expect that such a dependency would lead to a
536 difference in the time courses of the responses to positively and negatively skewed stimuli.

537 To test whether stimulus skewness has an effect on the cone kinetics, we compared impulse
538 response functions derived from the voltage responses to the -2.2 and the +2.2 “effective” skew
539 stimuli (Figure 8B). To better visualize the differences in kinetics we normalized these impulse
540 response functions by the amplitude of their initial lobe (Figure 8C). Interestingly, while on
541 average the cone impulse response functions peaked 3.6 ms (or $9 \pm 1.0 \%$) later for the

542 negatively skewed stimulus than for the positively skewed stimulus (Figure 8C, $p=0.0001$,
543 $n=7$), there were no statistically significant differences neither in its full width at the half
544 maximum (FWHM) ($\Delta = 1.0 \pm 1.35$ %; $p=0.37$; $n=7$), nor in the cone's integration time ($\Delta=$
545 1.1 ± 1.61 %; $p=0.51$; $n=7$).

546 **Discussion**

547 We studied responses of cone photoreceptors to differently skewed stimuli and found cone
548 response amplitudes to negatively skewed stimuli are up to 50% greater than to positively
549 skewed stimuli (Figures 2, 5A&C, 6A, 7). This amplitude difference originates from the
550 asymmetrical weighting of positive and negative contrasts by the phototransduction cascade.
551 Its gain is inversely proportional to Weber contrast steps raised to the power of -0.125 (Van
552 Hateren and Snippe, 2006; Figure 8A) and may serve as the basis for the Blackshot mechanism
553 proposed by Chubb et al. (1994, 2004). Additionally, we observed stimulus skewness changes
554 the cone's impulse response function shape. For the normalized impulse response function, the
555 rising flank was faster and the falling flank slower for positively compared to negatively
556 skewed stimuli (Figure 8C).

557 **The Blackshot mechanism**

558 Psychophysical studies reported that humans can discriminate visual stimuli based on skewness
559 (Chubb et al., 1994, 2004; Graham et al., 2016). Our results suggest that this discrimination
560 starts as early as the phototransduction cascade. Chubb et al. (1994, 2004) described the
561 sensitivity to skewness with the so-called Blackshot mechanism, which has a disproportionately
562 strong response to high negative contrasts. Our data indicates that differences in the response
563 to positively and negatively skewed stimuli originates in the phototransduction's asymmetric
564 gain function, which leads to higher response amplitudes to negative contrasts than to positive

565 contrasts (Figure 5C, Figure 8A). Moreover, in full accordance with psychophysical studies,
566 the difference in cone response amplitudes to positive and negative contrasts becomes more
567 prominent with larger contrast steps (Figure 8A). For the ± 1.6 “effective” skew stimuli pair,
568 where the maximal “effective” Weber contrast step was 0.5, the difference in the response was
569 about 15% while for the ± 2.2 “effective” skew pair, where the maximal “effective” Weber
570 contrast step was 0.8, the difference was almost 50% (Figure 5C).

571 Asymmetries in responses to positive and negative contrasts are reported throughout the entire
572 visual system in various species (Laughlin, 1981; Van Hateren, 1997; Lee et al., 2003; Zaghoul
573 et al., 2003; Jin et al., 2008; Yeh et al., 2009; Endeman and Kamermans, 2010; Baden et al.,
574 2013; Kremkow et al., 2014; Cooper and Norcia, 2015), including the human visual cortex
575 (Zemon et al., 1988; Kremkow et al., 2014). Although it was shown that differences in response
576 amplitudes to positive and negative contrasts are additionally amplified by the visual cortex
577 (Kremkow et al., 2014), our data clearly indicates that the primary origin of this asymmetry is
578 within the cone’s phototransduction cascade.

579 The phototransduction’s asymmetric gain function enables cones to efficiently encode the
580 entire range of contrasts present in natural scenes. Photoreceptors encode changes in their input
581 with a graded output. Information theory states that such a system encodes a signal efficiently
582 only when the statistical distribution of its output is Gaussian, which implies a symmetrical
583 engagement of the system’s dynamic range (Shannon, 1948; Van Hateren, 1997). On the other
584 hand, from a given mean, the light intensity cannot decrease by more than 100%, but can easily
585 increase by many orders of magnitude. This means that the dynamic range of positive contrasts
586 is wider than that of negative. Thus, although some visual scenes can be skewed negatively
587 (Tkačik et al., 2014), the total distribution of contrasts at any given intensity is skewed
588 positively with negative contrasts being smaller in amplitude, but more frequent than positive
589 contrasts (Laughlin, 1983; Ruderman, 1994; Van Hateren, 1997; Ruderman et al., 1998;

590 Cooper and Norcia, 2015). Consequently, to encode signals efficiently and to provide
591 symmetrical outputs, cones compensate for this asymmetry in their input by weighting high
592 positive contrasts with lower gain (Figure 8A), such that when stimulated with the entire range
593 of contrasts in natural scenes, cones provide a Gaussian output (Laughlin, 1983; Van Hateren,
594 1997; Endeman and Kamermans, 2010). We therefore suggest that the Blackshot mechanism
595 is simply a consequence of the more fundamental necessity to efficiently encode the range of
596 contrasts present in natural scenes.

597 **Shape of the impulse response function**

598 We found the cone's impulse response function peaks ≈ 3.6 ms later for negatively skewed
599 stimuli whereas the cone's integration time is unaffected by stimulus skewness (Figure 8B&C).
600 The rising and falling flanks of the cone's impulse response are governed by different
601 biophysical mechanisms. The former is heavily influenced by the phosphodiesterase (PDE)
602 hydrolysis of cGMP. The time constant of this process is inversely proportional to the light
603 intensity. Hence, it decreases upon positive, and increases upon negative contrast steps
604 (Nikonov et al., 2000; van Hateren, 2005; Endeman and Kamermans, 2010). The terminating
605 flank is largely regulated by the guanylyl cyclase (GC) mediated production of cGMP which
606 is modulated by the Ca^{2+} influx through the CNG channels. The time constant of this process
607 is not light-dependent but its gain is inversely proportional to the 4th power of light intensity
608 (Burns et al., 2002; van Hateren, 2005; van Hateren and Snippe, 2007). The interplay between
609 these two underlying processes is thought to account for the cone's impulse response function
610 shape, the asymmetric rising and falling response phases to sinusoidal stimuli, and for light
611 adaptation to decreases in light intensity being slower than for light intensity increases (Baylor
612 and Hodgkin, 1973; Lankheet et al., 1991; Nikonov et al., 2000; Lee et al., 2003; van Hateren,
613 2005; Endeman and Kamermans, 2010; Angueyra et al., 2021).

614 For our stimuli, the PDE hydrolysis of cGMP time-constant will have been shorter during
615 positively skewed stimuli as all large changes in light intensity were associated with positive
616 contrasts. This in turn manifest as a faster rate of change in the impulse response functions'
617 initial flank and hence an earlier time to peak. For negatively skewed stimuli, as all large
618 changes in light intensity were associated with negative contrast, GC mediated production of
619 cGMP was pronounced. The highly non-linear light-dependent gain function of this process,
620 and the ensuing Ca^{2+} influx when cones depolarized, increased the rate the cone CNG channels
621 reopened. This resulted in an increased decay rate for the terminating flank of the impulse
622 response function. Hence, the initial flank's faster onset rate during the positively skewed
623 stimulus is largely offset by the terminating flank's faster decay rate during the negatively
624 skewed stimulus. Consequently, the cone impulse response function integration time to
625 positive and negative skewed stimuli does not differ while it's time to peak does.

626 **Relation to previous studies using skewed stimuli**

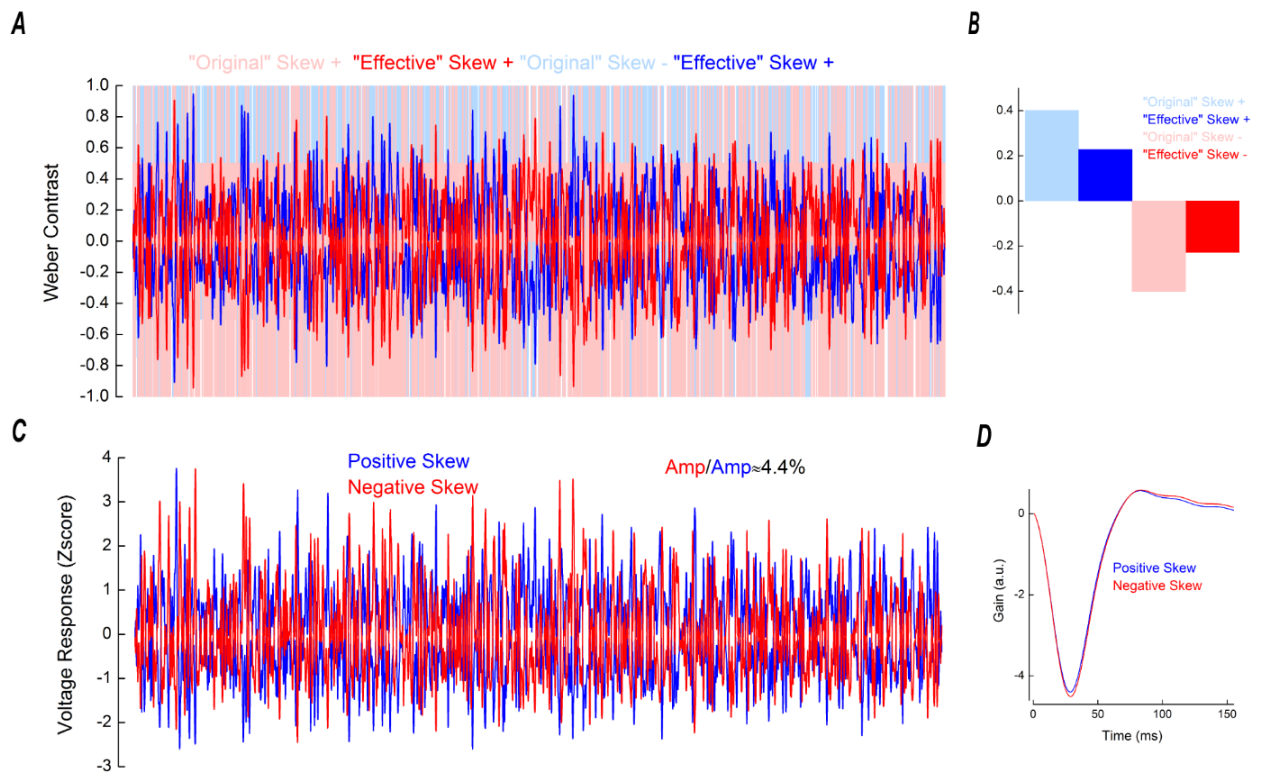
627 Why did previous studies find stimulus skewness had little to no effect on RGC (Tkačik et al.,
628 2014) and LGN neurons (Bonin et al., 2006)? We suggest a methodological factor. In both
629 studies, a large proportion of the stimulus power spectrum was outside the cone's temporal
630 frequency bandwidth. Indeed, Bonin et al. (2006) used white-noise stimuli bandlimited to 124
631 Hz to study cat LGN neurons responses, while the cat visual system barely responds to
632 frequencies above 32 Hz (Shapley and Victor, 1978; Mante et al., 2005). Similarly, Tkacik et
633 al. (2014) studied salamander RGC responses with white-noise bandlimited to 30 Hz, whereas
634 the salamander retina hardly reacts to frequencies above 10 Hz (Kim and Rieke, 2001). Thus,
635 in both these studies a large part of their stimuli were 'filtered out' and the remaining
636 "effective" stimuli were only able to elicit marginal skew dependent effects.

637 To illustrate this point, we estimated the "effective" stimuli delivered by Bonin et al. (2006)
638 and Tkacik et al. (2014) using Van Hateren's cone photoreceptor model (van Hateren and

639 Snippe, 2007). Simulations of the cat cone indicate that while a wide range of “effective”
640 Weber contrasts were present (Figure 9A) the “effective” skewness was approximately half
641 that of the original stimuli employed, reducing from a range of ± 0.4 to approximately ± 0.2
642 (Figure 9B). Hence, both stimuli delivered largely similar distributions of “effective” Weber
643 contrasts. As a result, the simulated voltage responses to the positive and negatively skewed
644 stimuli only differed in amplitude by approximately 4% (Figure 9 C, D), which is within the
645 range of standard error estimates for the amplitude differences we find here (Figure 5C).

646 Simulations of the salamander cone reveal a different situation that none the less leads to the
647 same outcome. The “effective” skewness range remained relatively large despite being less
648 than half that of the original stimuli employed (± 0.8 vs ± 2 , Figure 10B), but the range of
649 “effective” contrasts reduced to just ± 0.2 Weber unit (Figure 10A). Over this limited range of
650 contrasts the cone photoreceptor gain is mostly symmetrical (Figure 8A) and as such the
651 voltage response amplitude to the negatively skewed stimulus was only 2% higher than for the
652 positively skewed stimulus (Figure 10C&D). Hence, even though the stimuli had substantially
653 different distributions of “effective” Weber contrasts, the range of contrast values they
654 delivered were too narrow to generate a notable effect.

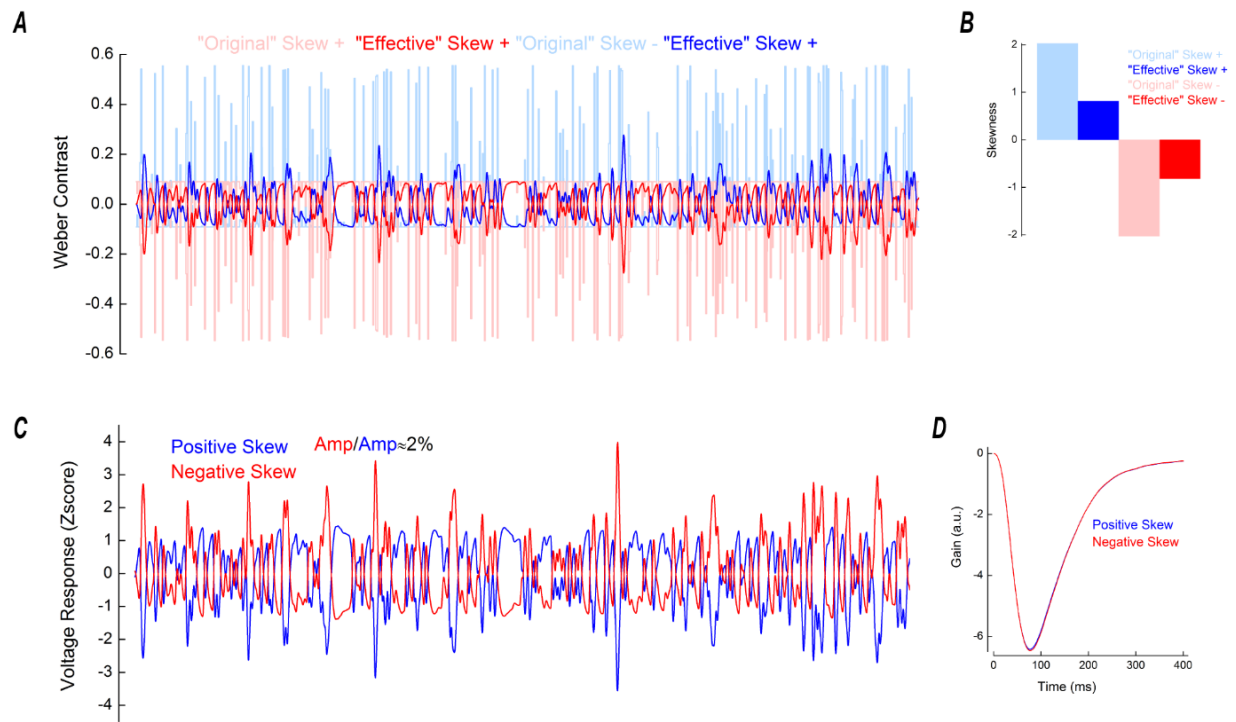
655 To conclude, our results show that to study visual processes under varying skewness
656 conditions, the stimuli must be able to deliver sufficient levels of “effective” skewness over
657 sufficient ranges of “effective” Weber contrasts.



658

659 **Figure 9**

660 Simulated responses of cat cone photoreceptors. **A.** Light blue and light red lines depict the positively and
 661 negatively skewed stimuli used by Bonin et al. (2006) and here for the simulation. Blue and red lines depict the
 662 “effective” positively and negatively skewed stimuli, obtained by the convolution of the “original” stimuli with
 663 the impulse response functions shown in **D.** **B.** Comparison of the skews of the “original” and “effective”
 664 positively (blue) and “negatively” (red) skewed stimuli. Due to the temporal filtering the “effective” stimuli are
 665 almost symmetrical around the mean, their skew range having decreased from ± 0.4 to $\approx \pm 0.2$. **C.** Simulated cone
 666 voltage responses to the positively (blue) and negatively (red) skewed stimuli. The response amplitude to the
 667 negatively skewed stimulus was 4% higher than the response amplitude to the positively skewed stimulus. The
 668 simulated voltage response amplitudes were quantified by their standard deviations, as for Figure 5C. Parameters
 669 for the simulation are listed in the Table 1. **D.** Impulse response functions derived from the simulated cat cone
 670 voltage responses. These impulse response functions were used to estimate the “effective” stimuli shown in **A.**



671

672 **Figure 10**

673 Simulated responses of salamander cone photoreceptors. **A.** Light blue and light red lines depict the positively
674 and negatively skewed stimuli used in the simulation. These stimuli had the same properties as those used by
675 Tkacik et al.(2014). Blue and red lines depict the “effective” positively and negatively skewed stimuli, obtained
676 by the convolution of the “original” stimuli with the impulse response functions shown in **D.** The temporal filtering
677 leads to small Weber contrast ranges of the “effective” stimuli. **B.** Comparison of the skews of the “original” and
678 “effective” positively (blue) and “negatively” (red) skewed stimuli. The salamander cone’s temporal filtering
679 reduced the stimulus skewness from ± 2 to ± 0.8 . **C.** Simulated cone voltage responses to the positively (blue) and
680 negatively (red) skewed stimuli. The response amplitude to the negatively skewed stimulus was 2% higher than
681 the response amplitude to the positively skewed stimulus. The simulated voltage response amplitudes were
682 quantified by their standard deviations, as for Figure 5C. Parameters for the simulation are listed in the Table 1.
683 **D.** Impulse response functions derived from the simulated salamander cone voltage responses. These impulse
684 response functions were used to estimate the “effective” stimuli shown in **A.**

685 **References**

686 Angueyra JM, Baudin J, Schwartz GW, Rieke F (2021) Multiple time scales of adaptation
687 allow cones to encode the inputs created by visual exploration of natural scenes.

688 bioRxiv:2021.02.13.431101.

689 Baccus SA, Meister M (2002) Fast and slow contrast adaptation in retinal circuitry. *Neuron*
690 36:909–919.

691 Baden T, Schubert T, Chang L, Wei T, Zaichuk M, Wissinger B, Euler T (2013) A tale of two
692 retinal domains: Near-Optimal sampling of achromatic contrasts in natural scenes through
693 asymmetric photoreceptor distribution. *Neuron* 80:1206–1217

694 Baylor DA, Hodgkin AL (1973) Detection and resolution of visual stimuli by turtle
695 photoreceptors. *J Physiol* 234:163–198

696 Bonin V, Mante V, Carandini M (2006) The statistical computation underlying contrast gain
697 control. *J Neurosci* 26:6346–6353.

698 Burns ME, Mendez A, Chen J, Baylor DA (2002) Dynamics of cyclic GMP synthesis in retinal
699 rods. *Neuron* 36:81–91.

700 Chichilnisky EJ (2001) A simple white noise analysis of neuronal light responses. *Netw*
701 *Comput Neural Syst* 12:199–213.

702 Chubb C, Econopouly J, Landy MS (1994) Histogram contrast analysis and the visual
703 segregation of IID textures. *J Opt Soc Am A* 11:2350.

704 Chubb C, Landy MS, Econopouly J (2004) A visual mechanism tuned to black. *Vision Res*
705 44:3223–3232.

706 Cooper EA, Norcia AM (2015) Predicting Cortical Dark/Bright Asymmetries from Natural
707 Image Statistics and Early Visual Transforms. *PLoS Comput Biol* 11:1–25.

708 Daly SJA, Normann R (1985) Temporal Information Processing In Cones: Effects of Light
709 Adaptation on Temporal Summation and Modulation. *Vision Res* 25:1197–1206.

- 710 Donner K, Hemila S (1996) Modelling the spatio-temporal modulation response of ganglion
711 cells with difference-of-Gaussians receptive fields: Relation to photoreceptor response
712 kinetics. *Vis Neurosci* 13:173–186.
- 713 Endeman D, Kamermans M (2010) Cones perform a non-linear transformation on natural
714 stimuli. *J Physiol* 588:435–446
- 715 Fahrenfort I, Habets RL, Spekreijse H, Kamermans M (1999) Intrinsic cone adaptation
716 modulates feedback efficiency from horizontal cells to cones. *J Gen Physiol* 114:511–524
- 717 Frazor RA, Geisler WS (2006) Local luminance and contrast in natural images. *Vision Res*
718 46:1585–1598.
- 719 Graham D, Schwarz B, Chatterjee A, Leder H (2016) Preference for luminance histogram
720 regularities in natural scenes. *Vision Res* 120:11–21
- 721 Howlett MHC, Smith RG, Kamermans M (2017) A novel mechanism of cone photoreceptor
722 adaptation. *PLoS Biol* 15:e2001210
- 723 Jin JZ, Weng C, Yeh CI, Gordon JA, Ruthazer ES, Stryker MP, Swadlow HA, Alonso JM
724 (2008) On and off domains of geniculate afferents in cat primary visual cortex. *Nat*
725 *Neurosci* 11:88–94.
- 726 Kamar S, Howlett MHC, Kamermans M (2019) Silent-substitution stimuli silence the light
727 responses of cones but not their output. *J Vis* 19:1–11.
- 728 Kamermans W, Ariette M, Farajnia S, Howlett M, Kamermans M (2017) A quantitative model
729 for adaptation of in cone photoreceptors to contrast.
- 730 Kim KJ, Rieke F (2001) Temporal contrast adaptation in the input and output signals of
731 salamander retinal ganglion cells. *J Neurosci* 21:287–299.

- 732 Korenberg MJ (1991) Parallel cascade identification and kernel estimation for nonlinear
733 systems. *Ann Biomed Eng* 19:429–455.
- 734 Kremkow J, Jin J, Kombar SJ, Wang Y, Lashgari R, Li X, Jansen M, Zaidi Q, Alonso JM
735 (2014) Neuronal nonlinearity explains greater visual spatial resolution for darks than
736 lights. *Proc Natl Acad Sci U S A* 111:3170–3175.
- 737 Lankheet MJM, van Wezel RJA, van de Grind WA (1991) Light adaptation and frequency
738 transfer properties of cat horizontal cells. *Vision Res* 31:1129–1142.
- 739 Laughlin S (1981) A simple coding procedure enhances a neuron's information capacity.
740 *Zeitschrift fur Naturforsch - Sect C J Biosci* 36:910–912.
- 741 Laughlin S (1983) Matching Coding to Scenes to Enhance Efficiency. :42–52.
- 742 Lee BB, Dacey DM, Smith VC, Pokorny J (2003) Dynamics of sensitivity regulation in primate
743 outer retina: The horizontal cell network. *J Vis* 3:513–526.
- 744 Malchow RP, Yazulla S (1986) Separation and light adaptation of rod and cone signals in the
745 retina of the goldfish. *Vision Res* 26:1655–1657.
- 746 Mante V, Frazor RA, Bonin V, Geisler WS, Carandini M (2005) Independence of luminance
747 and contrast in natural scenes and in the early visual system. *Nat Neurosci* 8:1690–1697
748 Available at: <http://www.nature.com/doi/10.1038/nn1556>.
- 749 Nikonov S, Lamb TD, Pugh EN (2000) The role of steady phosphodiesterase activity in the
750 kinetics and sensitivity of the light-adapted salamander rod photoresponse. *J Gen Physiol*
751 116:795–824
- 752 Rieke F (2001) Temporal contrast adaptation in salamander bipolar cells. *J Neurosci* 21:9445–
753 9454.

- 754 Ruderman DL (1994) The statistics of natural images. *Netw Comput Neural Syst* 5:517–548.
- 755 Ruderman DL, Cronin TW, Chiao C-C (1998) Statistics of cone responses to natural images:
756 implications for visual coding. *J Opt Soc Am A* 15:2036.
- 757 Schmitz Y, Witkovsky P (1997) Dependence of photoreceptor glutamate release on a
758 dihydropyridine- sensitive calcium channel. *Neuroscience* 78:1209–1216.
- 759 Shannon CE (1948) A Mathematical Theory of Communication. 27:379–423.
- 760 Shapley RM, Victor JD (1978) The effect of contrast on the transfer properties of cat retinal
761 ganglion cells. *J Physiol*:275–298.
- 762 Simoncelli EP, Pillow JW, Paninski L, Schwartz O (2004) Characterization of Neural
763 Responses with Stochastic Stimuli.
- 764 Student (1908) The probable Error of a Mean. *Biometrika* 6:1–25.
- 765 Thoreson WB, Rabl K, Townes-Anderson E, Heidelberger R (2004) A highly Ca²⁺-sensitive
766 pool of vesicles contributes to linearity at the rod photoreceptor ribbon synapse. *Neuron*
767 42:595–605.
- 768 Tkačik G, Ghosh A, Schneidman E, Segev R (2014) Adaptation to changes in higher-order
769 stimulus statistics in the salamander retina. *PLoS One* 9.
- 770 van Hateren H (2005) A cellular and molecular model of response kinetics and adaptation in
771 primate cones and horizontal cells. *J Vis* 5:331–347.
- 772 Van Hateren JH (1997) Processing of natural time series of intensities by the visual system of
773 the blowfly. *Vision Res* 37:3407–3416.
- 774 Van Hateren JH, Rüttiger L, Sun H, Lee BB (2002) Processing of natural temporal stimuli by
775 macaque retinal ganglion cells. *J Neurosci* 22:9945–9960.

- 776 van Hateren JH, Snippe HP (2007) Simulating human cones from mid-mesopic up to high-
 777 photopic luminances. *J Vis* 7:1.
- 778 Van Hateren JH, Snippe HP (2006) Phototransduction in primate cones and blowfly
 779 photoreceptors: Different mechanisms, different algorithms, similar response. *J Comp*
 780 *Physiol A Neuroethol Sensory, Neural, Behav Physiol* 192:187–197.
- 781 Vroman R, Klaassen LJ, Howlett MHC, Cenedese V, Klooster J, Sjoerdsma T, Kamermans M
 782 (2014) Extracellular ATP Hydrolysis Inhibits Synaptic Transmission by Increasing pH
 783 Buffering in the Synaptic Cleft. *PLOS Biol* 12:e1001864
- 784 Welch PD (1967) Welch's Periodogram.pdf. *IEEE Trans Audio Electroacoust* 15:70–73.
- 785 Wiener N (1964) Extrapolation, Interpolation, and Smoothing of Stationary Time Series. The
 786 MIT Press.
- 787 Yeh CI, Xing D, Shapley RM (2009) “Black” responses dominate macaque primary visual
 788 cortex V1. *J Neurosci* 29:11753–11760.
- 789 Zaghloul KA, Boahen K, Demb JB (2003) Different circuits for ON and OFF retinal ganglion
 790 cells cause different contrast sensitivities. *J Neurosci* 23:2645–2654.
- 791 Zemon V, Gordon J, Welch J (1988) Asymmetries in ON and OFF visual pathways of humans
 792 revealed using contrast-evoked cortical potentials. *Vis Neurosci* 1:145–150.

793

794 **Table 1**

Parameter	Goldfish	Cat	Salamander
Lifetime of activated conopsin	8 – 31 ms	8 ms	88 ms
Lifetime of activated transducin	16 – 30 ms	12 ms	101 ms
Dark PDE activity	0.003 ms ⁻¹	0.0028 ms ⁻¹	0.003 ms ⁻¹
Constant of the dependence of PDE activity on transducin activation	0.00004 0.00023	-	0.00016 0.0002

Apparent Hill coefficient of CNG channels	1	1	1
Hill coefficient of GC activation	4	4	4
Time constant of calcium extrusion	12 -28 ms	9 ms	24 ms
GC activation constant	0.1	0.09	0.1
Capacitive membrane time constant	15 ms	6 ms	15 ms
Parameter of membrane non-linearity	0.7 – 1.1	0.8	0.85
Constant of membrane nonlinearity	0.03 – 0.07	0.07	0.085
Time constant of membrane non-linearity	300 ms	120 ms	300 ms

795

796 Parameters of the Van Hateren model used to simulate the responses of goldfish, salamander

797 and cat cones. For the goldfish, model parameters were obtained by fitting cones responses

798 (n=7) to Skew Stimulus Set #2 while constraining the range the parameters varied to within

799 that determined by Endeman and Kamermans (2010). For the cat and salamander, parameters

800 were adjusted such that the simulated-cone's impulse response function time-to-peak

801 approximately matched that estimated, respectively, by Donner and Hemila (1996) and by

802 Rieke (2001) and Baccus and Meister (2002).